Katanin maintains meiotic metaphase chromosome alignment and spindle structure in vivo and has multiple effects on microtubules in vitro

Karen McNally[a], Evan Berg[a], Daniel B. Cortes[a], Veronica Hernandez[a], Paul E. Mains[b], and Francis J. McNally[a]

[a]Department of Molecular and Cellular Biology, University of California, Davis, Davis, CA 95616; [b]Genes and Development Research Group, Department of Biochemistry and Molecular Biology, University of Calgary, Calgary, AB T2N 4N1, Canada

ABSTRACT **Assembly of *Caenorhabditis elegans* female meiotic spindles requires both MEI-1 and MEI-2 subunits of the microtubule-severing ATPase katanin. Strong loss-of-function mutants assemble apolar intersecting microtubule arrays, whereas weaker mutants assemble bipolar meiotic spindles that are longer than wild type. To determine whether katanin is also required for spindle maintenance, we monitored metaphase I spindles after a fast-acting *mei-1(ts)* mutant was shifted to a nonpermissive temperature. Within 4 min of temperature shift, bivalents moved off the metaphase plate, and microtubule bundles within the spindle lengthened and developed a high degree of curvature. Spindles eventually lost bipolar structure. Immunofluorescence of embryos fixed at increasing temperature indicated that MEI-1 was lost from spindle microtubules before loss of ASPM-1, indicating that MEI-1 and ASPM-1 act independently at spindle poles. We quantified the microtubule-severing activity of purified MEI-1/MEI-2 complexes corresponding to six different point mutations and found a linear relationship between microtubule disassembly rate and meiotic spindle length. Previous work showed that katanin is required for severing at points where two microtubules intersect in vivo. We show that purified MEI-1/MEI-2 complexes preferentially sever at intersections between two microtubules and directly bundle microtubules in vitro. These activities could promote parallel/antiparallel microtubule organization in meiotic spindles.**

Monitoring Editor
Stephen Doxsey
University of Massachusetts

Received: Jan 2, 2014
Revised: Jan 27, 2014
Accepted: Jan 28, 2014

INTRODUCTION

The microtubule-severing enzyme katanin is widely conserved among eukaryotes and plays diverse roles in a number of cellular processes. Katanin was originally purified from sea urchin eggs based on its ATP-dependent microtubule-severing activity and consists of a heterodimer composed of a 60-kDa catalytic subunit and an 80-kDa accessory subunit (McNally and Vale, 1993; Hartman *et al.*, 1998). The catalytic subunit is a member of a family of closely related AAA ATPases and has been shown to have microtubule-binding and microtubule-severing activity in the absence of the accessory subunit (Hartman and Vale, 1999; Stoppin-Mellet *et al.*, 2007; Eckert *et al.*, 2012). The cellular function of the accessory subunit has remained elusive; however, genomes of eukaryotes that contain katanin catalytic subunits invariably contain katanin accessory subunits, and mutations in the accessory subunits cause the same phenotype as mutations in catalytic subunits in *Caenorhabditis elegans* (Mains *et al.*, 1990), *Tetrahymena* (Sharma *et al.*, 2007), and *Chlamydomonas* (Dymek *et al.*, 2004; Dymek and Smith, 2012). These observations suggest that the cellular activity of katanin absolutely requires a complex of both subunits.

This article was published online ahead of print in MBoC in Press (http://www.molbiolcell.org/cgi/doi/10.1091/mbc.E13-12-0764) on February 5, 2014.

Address correspondence to: Francis J. McNally (fjmcnally@ucdavis.edu).

Abbreviations used: BSA, bovine serum albumin; DAPI, 4′,6-diamidino-2-phenylindole; EGTA, ethylene glycol tetraacetic acid; GFP, green fluorescent protein; IgG, immunoglobulin G; PBS, phosphate-buffered saline; PBST, PBS containing 0.05% Tween 20; RNAi, RNA interference; ts, temperature-sensitive.

In *C. elegans*, the katanin p60 catalytic subunit MEI-1 and the accessory subunit MEI-2 are required for the formation of female meiotic spindles (Mains *et al.*, 1990) and are concentrated at meiotic spindle poles and chromosomes (Clark-Maguire and Mains, 1994a; Srayko *et al.*, 2000; McNally *et al.*, 2006). Wild-type oocyte meiotic spindles are composed of dense parallel/antiparallel microtubule bundles (McNally *et al.*, 2006; Wignall and Villeneuve, 2009) composed of very short microtubules (Srayko *et al.*, 2006). *mei-1(null)* spindles contain only very long microtubules (Srayko *et al.*, 2006) that are assembled around chromosomes as apolar arrays of intersecting microtubules (Mains *et al.*, 1990; McNally and McNally, 2011). Weaker alleles of both *mei-1* and *mei-2* promote the assembly of meiotic spindles that are bipolar but longer than wild type (McNally *et al.*, 2006; McNally and McNally, 2011; Gomes *et al.*, 2013). The length of these spindles is stable during metaphase, suggesting that weak *mei-1* and *mei-2* alleles might only affect spindle length during the assembly stage.

Katanin might promote the formation of parallel/antiparallel microtubule bundles and bipolar meiotic spindles by several not mutually exclusive mechanisms. Microtubule severing might promote parallel/antiparallel structures simply by shortening microtubules, and short microtubules may bundle more efficiently, because they can pivot, diffuse, or be transported more quickly. Alternatively, katanin might promote parallel/antiparallel microtubule formation by selectively severing microtubules at the intersections where two microtubules cross each other, a phenomenon observed in vivo in specific cell types of *Arabidopsis* (Wightman and Turner, 2007; Lindeboom *et al.*, 2013; Zhang *et al.*, 2013). A third possibility is that katanin directly cross-bridges microtubules to promote the formation of microtubule bundles. In this study, we utilized a fast-acting *mei-1(ts)* mutant to explore whether katanin activity is required to maintain spindle structure. We found that MEI-1/MEI-2 complexes are required continuously in vivo to maintain chromosome position, spindle length, and parallel/antiparallel microtubule organization. We also analyzed the in vitro activities of MEI-1/MEI-2 complexes to rigorously test the relationship between microtubule severing and meiotic spindle length.

RESULTS

Rapid inactivation of katanin during metaphase causes chromosome misalignment associated with lengthening and bending of spindle fibers

Previous studies of meiotic spindle defects in *mei-1* and *mei-2* mutants (Mains *et al.*, 1990; Yang *et al.*, 2003; McNally *et al.*, 2006; McNally and McNally, 2011; Srayko *et al.*, 2006) were of spindles assembled in the absence of wild-type MEI-1/MEI-2. To test whether the activity of MEI-1/MEI-2 is also required continuously to maintain structure after spindle assembly, we did temperature-shift experiments with a fast-acting temperature-sensitive (ts) mutant, *mei-1(or642)* (O'Rourke *et al.*, 2011). Embryos within the uterus of *mei-1(or642)* worms grown at 16°C were arrested after spindle assembly at metaphase I by depletion of a component of the anaphase-promoting complex *mat-1* (Davis *et al.*, 2002) by RNA interference (RNAi). The embryos were initially imaged on a temperature-controlled stage set at the permissive temperature of 20°C; the temperature control setting was then quickly shifted to 25°C. Time-lapse imaging of green fluorescent protein (GFP)::tubulin and mCherry::histone revealed that in 8/11 *mei-1(or642); mat-1(RNAi)* embryos, chromosomes moved off the metaphase plate within 4 min of temperature shift (Figure 1C, 3′30″). The pole–pole spindle length increased from 8.63 ± 0.14 µm to 9.53 ± 0.36 µm (n = 11). The shape of individual microtubule bundles changed constantly during the 10 min of observation (illustrated for four consecutive, 15-s time points in Figure 1D). Some individual bundles developed a high degree of curvature resulting in some bundles bending out of the focal plane (dark region at 7′45″ in Figure 1C). At late time points, spindle fibers splayed outward from the central spindle in 8/11 embryos (arrow at 6′15″ in Figure 1C). The splayed fibers had a length indicating they extended past the spindle midpoint before splaying out of the spindle. Finally, in 6/11 *mei-1(or642)* spindles, it appeared that one or both poles had come apart, however, as discussed below, this was difficult to document by live imaging (Figure 1C, 11′). A plot of spindle length versus time shows a metaphase spindle growing for the first 3.5 min after the temperature shift, then decreasing in pole-to-pole length as the spindle fibers bend, and finally decreasing dramatically in length as one spindle pole breaks (Figure 1E). In contrast, 10/10 metaphase-arrested, wild-type spindles maintained a constant shape, length, and chromosome position during the ~11 min monitored after temperature shift to 25°C (pole-to-pole spindle length: 8.11 ± 0.19 µm at 0 min, 8.12 ± 0.18 µm at 10 min; Figure 1, A and D). *mei-1(or642)* spindles maintained at 20–21°C exhibited an intermediate phenotype, lengthening modestly from 8.46 ± 0.26 µm at 0 min to 8.84 ± 0.33 µm at 10 min (n = 9; Figure 1B). These results indicated that katanin acts continuously during metaphase to prevent lengthening of microtubule bundles and splaying of microtubule bundles out from the midzone and to maintain metaphase chromosome positioning.

Point mutations in MEI-1 and MEI-2 reveal a linear relationship between in vitro microtubule-disassembly activity and in vivo meiotic spindle length

To test the relationship between microtubule-severing activity and meiotic spindle length more rigorously, we quantified microtubule-disassembly activities of four viable and two lethal MEI-1 or MEI-2 point mutants (Table 1). Untagged 1:1 complexes of wild-type MEI-1 and MEI-2 were first purified (Figure 2A) and shown to sever Taxol-stabilized microtubules in vitro in the presence of ATP and to depolymerize microtubules from both severed ends (Figure 2, B–D). To quantify the rate of microtubule disassembly, we determined the average pixel value of all the microtubules in a field of view (typically > 100 microtubules and > 3000 µm of total microtubule length, e.g., Figure 2C) for each frame of a time-lapse sequence, background subtracted and normalized to 100% in the first frame. A plot of normalized fluorescence intensity over time for a single reaction (Figure 2E) revealed a lag period of 50 s followed by a fast linear phase and then a plateau caused by substrate depletion. The slope of the fast linear phase, which corresponds to the rate of removal of tubulin subunits from the lattice, was averaged from multiple assays from two independent preparations of wild-type MEI-1/MEI-2 (Table 1 and Figure 2F). The small variation in rate between assays utilizing independent preparations of protein and the linear relationship between disassembly rate and MEI-1/MEI-2 concentration (Table 1 and Figure 2F) justified a quantitative comparison of the disassembly rates for different point mutations isolated as intragenic suppressors of the dominant *mei-1* allele, *ct46* (Mains *et al.*, 1990; Clandinin and Mains, 1993). Two independent preparations for each mutant were normalized to the same concentration of MEI-1 (Figure 2G), and microtubule disassembly rates from multiple assays were averaged (Table 1). A plot of metaphase I spindle length (Table 2; McNally *et al.*, 2006; McNally and McNally, 2011) against microtubule disassembly rate at 0.187 µM MEI-1/MEI-2 revealed a linear relationship with an R2 of 0.89 (Figure 2H). This result strongly supports the hypothesis that the microtubule disassembly activity of

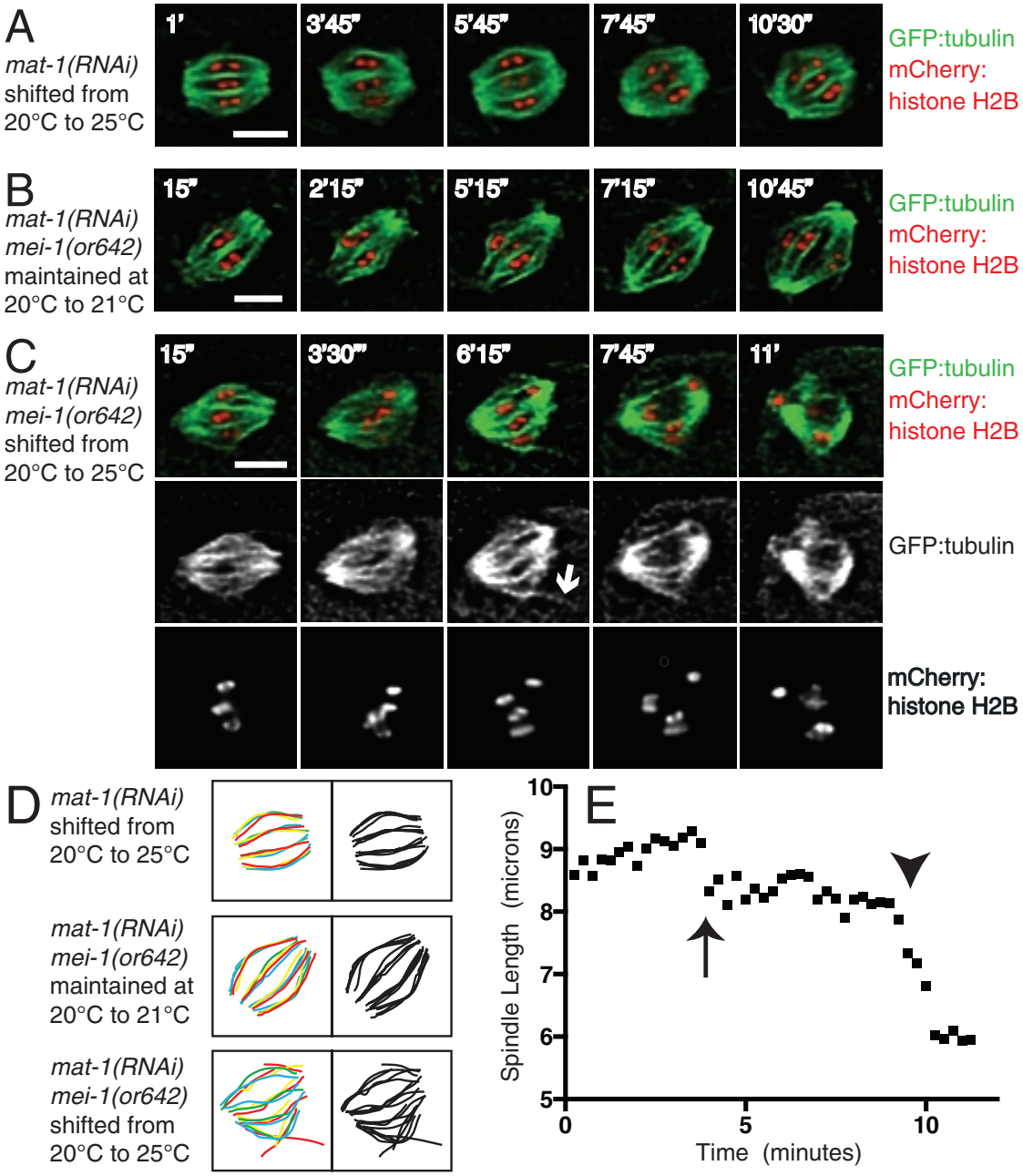

FIGURE 1: MEI-1 is required for maintenance of metaphase meiotic chromosome position and spindle structure. Metaphase-arrested *mat-1(RNAi)* and *mat-1(RNAi) mei-1(or642)* embryos expressing GFP::tubulin and mCherry::histone were grown at 16°C and imaged on a temperature-controlled microscope stage initially set at 20°C. After the first image was captured, the temperature was either shifted to 25°C for (A) and (C) or maintained at 20–21°C for (B). Images were captured at 15-s intervals for 10–11 min. Imaged spindles were in the +1 embryo, i.e., the most recently fertilized embryo in the uterus. (A) *mat-1(RNAi)*. (B) *mat-1(RNAi) mei-1(or642)*. (C) *mat-1(RNAi) mei-1(or642)* shifted to 25°C. Scale bars: 5μm. (D) For documentation of spindle fiber mobility, spindle fibers were traced in four consecutive images captured 5–7 min after the start of filming. The order of the tracings was blue, green, yellow, and, finally, red. Tracings were overlapped in their respective colors and also in black. (E) The pole-to-pole length of the spindle imaged in (C) was measured for each time point. An arrow indicates the time when the spindle begins to bend; an arrowhead indicates the time when one pole began to come apart.

MEI-1/MEI-2 limits the length of microtubules within spindle fibers during meiotic metaphase.

Strikingly, the *y*-intercept of the plot in Figure 2H predicts a spindle length of only 134% of wild type at a severing rate of zero. However, inviable mutants with no detectable in vitro microtubule-severing activity, such as *mei-1(b284)* and *mei-2(ct46ct82)* (Table 1), instead form completely apolar structures that lack any discrete focus of the spindle pole marker ASPM-1 (Table 3; McNally and McNally, 2011). Importantly, MEI-1(*b284*) is present at wild-type concentrations as assayed by immunoblotting (McNally and McNally, 2011), and the potent dominant lethality caused by *mei-1(ct46ct82)* (Mains *et al.*, 1990) indicates that the protein is

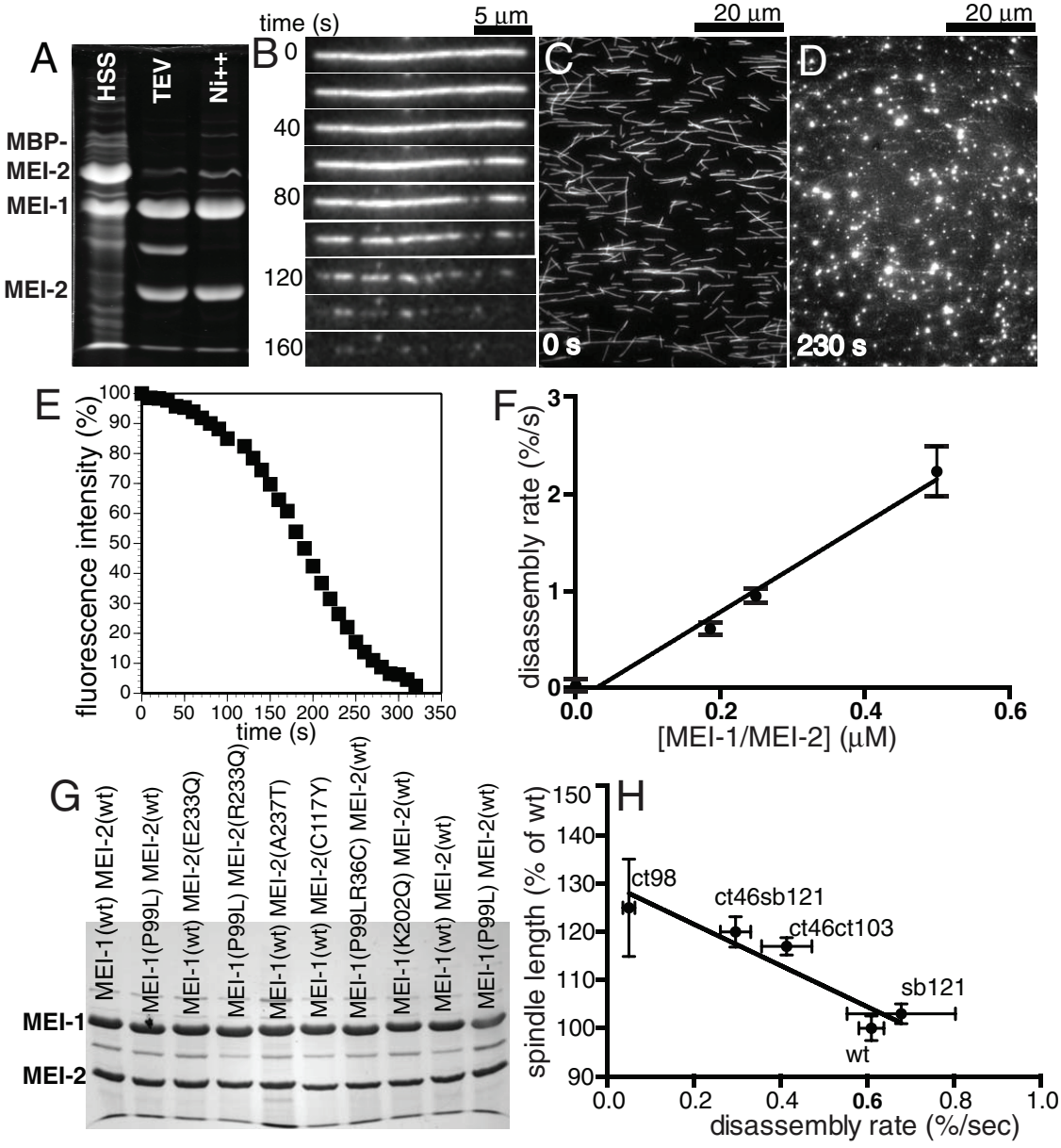

FIGURE 2: A linear relationship between in vitro microtubule disassembly rates and in vivo spindle length. (A) The untagged short isoform of MEI-1 was coexpressed with MBP-TEV-MEI-2 in *E. coli* and purified by amylose affinity chromatography, eluted with TEV protease, resolved by SDS–PAGE, and then stained with Coomassie Brilliant Blue G250. hss, high-speed supernatant of *E. coli* lysate; TEV, TEV elution from amylose column; Ni++, elution of TEV fraction from Ni^{2+} chelate column. Untagged MEI-2 binds to Ni^{2+} chelate columns. Ni^{2+}-purified MEI-1/MEI-2 was used only in Figure 6, B and C. (B–D) Fluorescence micrographs of Taxol-stabilized microtubules assembled from rhodamine-labeled porcine tubulin and immobilized in a flow cell. (B) Time-lapse images of a single microtubule undergoing MEI-1/MEI-2–dependent severing and depolymerization from the sites of internal breakage. (C, D) Representative images of an entire field of view used to quantify the average pixel value of all the microtubules during time-lapse imaging. Bright spots at 230 s are tubulin aggregates generated during the reaction. (E) Representative plot of background-subtracted average pixel values of all of the microtubules in a field of view scaled to 100% in the first frame. (F) Rates of microtubule disassembly determined from the linear phase of plots like that shown in (E) show a linear relationship with MEI-1/MEI-2 concentration. (G) Representative Coomassie Brilliant Blue G250–stained SDS–PAGE of different MEI-1 and MEI-2 point mutants purified from *E. coli* showing equalized concentration. (H) Microtubule disassembly rates of four different MEI-1/MEI-2 mutants from Table 1 plotted against metaphase I spindle length expressed as percent of wild type. Spindle length data were taken from Table 2, McNally *et al*. (2006), and McNally and McNally (2011). Expression levels for these mutants were shown in McNally and McNally (2011) and Srayko *et al*. (2000).

present in vivo. To investigate the strong, apolar spindle phenotype in more detail, we analyzed temperature-shifted *mei-1(or642ts)* embryos by fixed immunofluorescence with anti–ASPM-1 and anti–MEI-1 antibodies.

Rapid inactivation of katanin results in complete loss of ASPM-1 positive spindle poles

During live in utero imaging of temperature-shifted *mei-1(or642)* embryos, the *mei-1(null)* apolar spindle phenotype was not

MEI-1 (short)	MEI-2	[μM]	Severing rate (%/s)	SEM	*n*
None		0	0.023	0.002	3
wt	*wt*	0.187	0.61	0.03	5
wt	*wt*	0.25	0.95	0.02	4
wt	*wt*	0.5	2.24	0.26	4
ct46	*wt*	0.187	0.55	0.11	4
wt	*sb121*	0.187	0.68	0.13	4
ct46	*sb121*	0.187	0.29	0.035	4
ct46ct103	*wt*	0.187	0.41	0.06	4
wt	*ct98*	0.187	0.049	0.014	4
b284	*wt*	0.5	0.034	0.03	2
ct46ct82	*wt*	0.5	0.025	0.017	2

MEI-1(short) indicates the shorter of two alternatively spliced *mei-1* mRNAs (Clark-Maguire and Mains, 1994b). [μM] indicates the concentration of MEI-1. The severing rate for a single flow cell is the rate of decrease in the average fluorescence intensity of all the microtubules in a field of view normalized to 100% in the first frame. Severing rates shown are the average rate from multiple flow cells. *n* = number of flow cells.

TABLE 1: In vitro microtubule-disassembly rates of MEI-1/MEI-2 complexes.

Genotype	MI spindle length (μm)[a]	Number of spindles
mei-1(+) mei-2(+)	8.10 ± 0.15	12
mei-1(ct46) mei-2(+)	7.46 ± 0.15	8
mei-1(+) mei-2(sb121)	8.39 ± 0.09	11
mei-1(ct46), mei-2(sb121) reconstructed	9.55 ± 0.25	12

[a]Metaphase I spindle lengths were determined from time-lapse sequences of GFP::tubulin–labeled meiotic spindles filmed in utero. Only spindles that maintained a constant length for at least 3 min were used.

TABLE 2: Metaphase I spindle lengths.

rigorously documentable for two possible reasons. First, the mounting arrangement for in utero imaging makes it impossible to measure the temperature at the worm, and thus it is possible that the worm did not reach 25°C until late during the 10-min observation period. Second, metaphase spindles often move, even as they are anchored at the cortex, and a spindle pole that moves into an odd orientation relative to the focal plane can be difficult to image and mistaken for a missing spindle pole. Both limitations were circumvented in fixed immunofluorescence experiments because worms were temperature shifted by transfer to a large volume of buffer at the appropriate temperature and because complete Z stacks could be captured of fixed spindles stained with anti–ASPM-1 antibody. Fixed embryos were not *mat-1* arrested because the length of arrest cannot be estimated for embryos that have been removed from the uterus and prolonged metaphase arrest causes severe spindle and chromosome defects (Sonneville and Gönczy, 2004). Only spindles that were bipolar before the temperature shift were included in the sample. Such spindles were easily distinguished from spindles assembled during the temperature shift, because MEI-1 is required for translocation of metaphase spindles to the cortex, and thus spindles assembled in the absence of MEI-1 are located internally (Yang *et al.*, 2003). One hundred percent of embryos in worms grown at 16°C and shifted to 25°C for 10 min lacked ASPM-1–positive spindle poles (Figure 3A and Table 4). These spindles also completely lacked MEI-1 protein (Figure 3B and Table 4). This result indicates that bipolar spindles assembled at 16°C completely collapsed into apolar *mei-1(null)* structures in *mei-1(or642)* embryos at 25°C. Thus MEI-1 is required for maintenance of metaphase spindle poles.

The relationship between MEI-1/MEI-2 and ASPM-1 is likely indirect

ASPM-1 is found at *C. elegans* acentriolar meiotic spindle poles, where it is required for targeting of LIN-5 and dynein to spindle poles (van der Voet *et al.*, 2009). The findings that ASPM-1 foci are lost upon temperature shift of *mei-1(or642)* (Figure 3 and Table 4) and that ASPM-1 foci are absent from lethal alleles of *mei-1* or *mei-2* (McNally and McNally, 2011; Table 3) suggests that MEI-1/MEI-2 might directly target ASPM-1 to spindles. However, in *mei-1(or642)* embryos shifted to 16 or 20°C for 10 min, the concentration of MEI-1 on spindle poles was 37% that of wild type, whereas the concentration of ASPM-1 at

Genotype	Bipolar	Average pixel intensity of α-tubulin spindle/cytoplasm	Average pixel intensity of MEI-1 spindle/cytoplasm	Average pixel intensity of ASPM spindle/cytoplasm	Embryos with MEI-1on chromosomes
mei-1(+) mei-2(+)	Yes	4.93 ± 0.42 *n* = 14	2.56 ± 0.33 *n* = 14	2.42 ± 0.32 *n* = 14	16/16
mei-1(+) mei-2(ct98)	Yes	3.49 ± 0.31 *n* = 14	1.25 ± 0.08 *n* = 14	n.d.	10/14
mei-1(+) mei-2(ct102)	No	3.03 ± 0.33 *n* = 12	1.14 ± 0.04 *n* = 12	1.21 ± 0.30 *n* = 12	0/12
mei-1(ct46ct101) mei-2(+)	No	2.24 ± 0.10 *n* = 14	0.87 ± 0.04 *n* = 14	n.d.	0/14
mei-1(b284) mei-2(+)	No	2.96 ± 0.53 *n* = 8	1.12 ± 0.05 *n* = 9	1.21 ± 0.04 *n* = 8	0/9

Embryos from worms with the indicated genotypes were fixed and stained either with anti–MEI-1 and anti-tubulin antibodies or with anti–ASPM-1 and anti-tubulin antibodies.

TABLE 3: MEI-1 and ASPM-1 localization on meiotic spindles of strong *mei-1* and *mei-2* alleles.

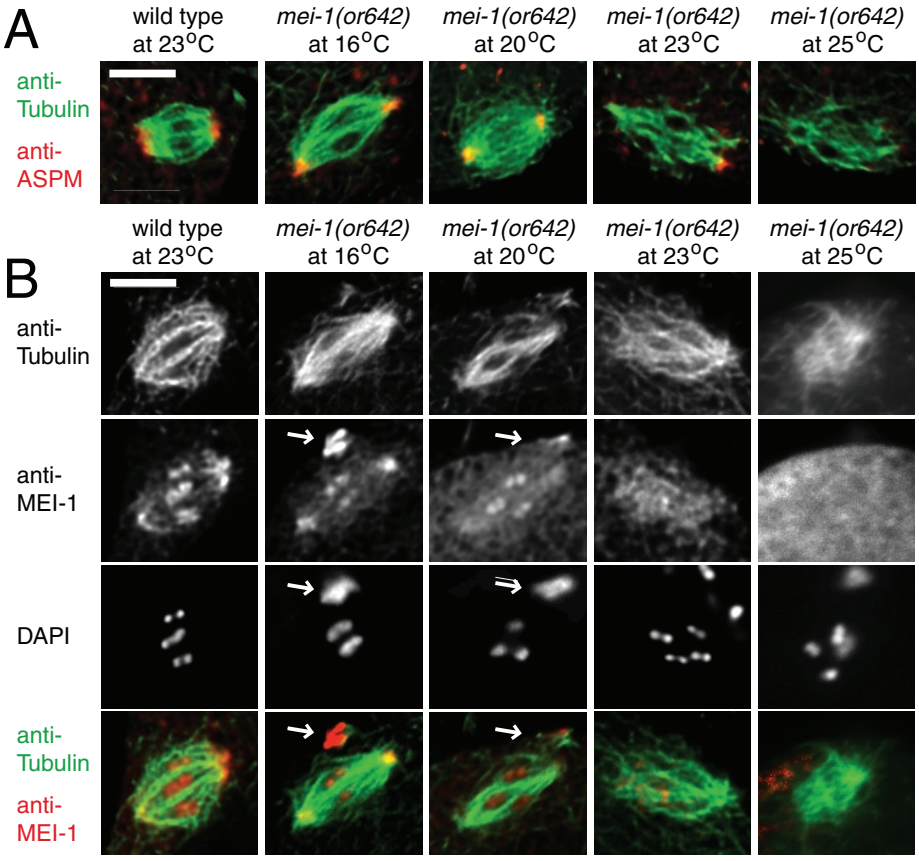

FIGURE 3: Increased incubation temperature of *mei-1(or642)* worms results in depletion of MEI-1 and ASPM-1 from metaphase meiotic spindles, chromosome mispositioning, and loss of organized parallel microtubule structure. (A) Images of metaphase spindles from wild type incubated for 10 min at 23°C and from *mei-1(or642)* incubated for 10 min at the temperatures shown. Embryos were fixed and stained with anti–ASPM-1 (red), anti-tubulin (green), and DAPI. Scale bar: 5 μm. (B) Images of metaphase spindles from embryos incubated and fixed as in (A) and stained with anti–MEI-1 (red), anti-tubulin (green), and DAPI. Scale bar: 5 μm. Arrows indicate the position of polar bodies.

spindle poles was unaffected at these temperatures (Table 4 and Figure 3). In contrast, displacement of chromosomes from the metaphase plate was already severe at 20°C (Table 4). These results suggest that ASPM-1 is not targeted to spindles by direct binding to MEI-1/MEI-2 and that loss of ASPM-1 from *mei-1* mutant spindles is not the cause of the chromosome-alignment phenotype.

For further investigation of the relationship between ASPM-1 and katanin, *aspm-1(RNAi)* meiotic spindles were stained with anti–MEI-1 or, as a control, anti-ASPM (Figure 4, A and B). No labeling of spindles with anti-ASPM was observed, indicating that the RNAi-mediated depletion of ASPM was complete. ASPM-1–depleted spindles had very elongated, pointed spindle poles that retained strong anti–MEI-1 staining, suggesting that MEI-1/MEI-2 might hold spindle poles together in the absence of ASPM-1. For further examination of this hypothesis, *mei-1(or642)* embryos were depleted of ASPM-1 and imaged at the intermediate temperature of 20°C. Of the double-mutant spindles, 17/17 had no bipolar structure (Figure 4C) compared with 9/9 *mei-1(or642)* single-mutant spindles, which retained bipolar structure at 20°C (Figure 1B), suggesting the limited MEI-1 activity in these embryos was not sufficient to maintain spindle poles in the absence of ASPM-1. These results suggest that katanin acts before and independently of ASPM-1, because, in the absence of ASPM, katanin-bound spindle poles were present, whereas, in conditions in which katanin was limited or absent, no spindle poles or ASPM-1 localization were observed.

Progressive loss of katanin leads to a progressive loss in the organization of pole-to-pole microtubule bundles

Wild-type metaphase spindles are composed of microtubule bundles that extend from pole to pole and have extremely uniform thickness, brightness, and spacing between bundles (Figures 1A, 3B, and 5A). The spaces between the bundles are occupied by chromosomes, and the bundles completely ensheathe chromosomes, as there is uniform tubulin intensity around each chromosome viewed down the pole-to-pole axis (Figure 5B). The regularity in bundle thickness and spacing is clearly seen for wild type in the intensity plot shown in Figure 5A. After *mei-1(or642)* embryos were shifted to increasing temperatures, pole-to-pole bundles became wider, and the spacing

Strain	Tubulin spindle/ cytoplasm	MEI-1 spindle/ cytoplasm	Percent spindles with all bivalents at metaphase plate	*n*	ASPM-1 spindle/ cytoplasm	*n*
Wild type 23°C	4.93 ± 0.42	2.56 ± 0.33	92.9	14	1.47 ± 0.11	11
mei-1(or642) 16°C	4.98 ± 0.56	1.80 ± 0.18	66.7	12	1.42 ± 0.07	11
mei-1(or642) 20°C	4.80 ± 0.43	1.58 ± 0.08	23.5	17	1.45 ± 0.05	12
mei-1(or642) 23°C	4.27 ± 0.41	1.25 ± 0.04	0	17	1.16 ± 0.03	11
mei-1(or642) 25°C	3.41 ± 0.31	1.06 ± 0.05	0	15	1.03 ± 0.02	11
mei-1(null)	2.45 ± 0.13	0.93 ± 0.04	0	14	n.d.	n.d.

mei-1(or642) worms were shifted from 16°C to increasing temperatures for 10 min before embryos were dissected, fixed, and stained with either anti-tubulin and anti–MEI-1 antibodies or with anti–ASPM-1 and anti-tubulin antibodies.

TABLE 4: MEI-1 and ASPM-1 staining intensities on *mei-1(or642)* meiotic spindles at increasing temperatures.

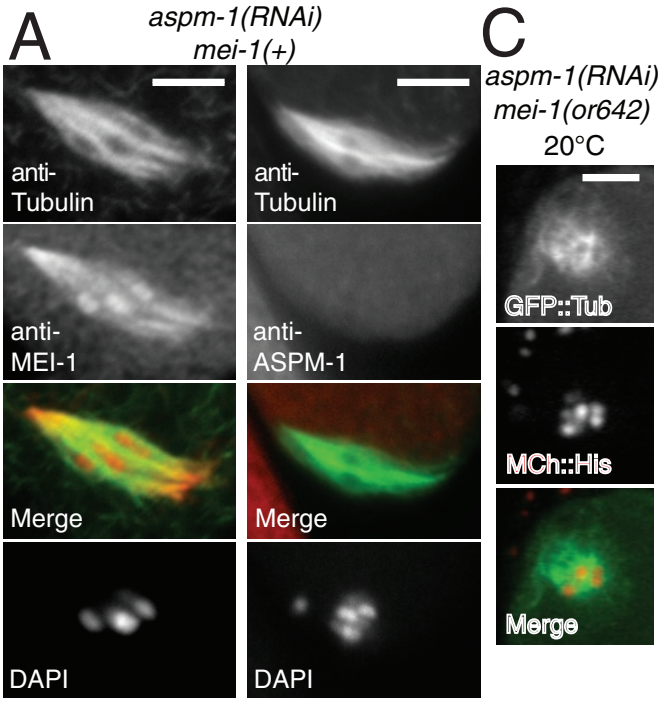

B

Stain	Average Pixel Intensity Spindle/Cytoplasm	N
anti-MEI-1	2.11 +/- 0.14	14
anti-ASPM-1	0.99 +/- 0.04	14

FIGURE 4: MEI-1 localizes to spindle poles and is required for spindle pole formation in the absence of ASPM-1. (A) RNAi by feeding beginning at the L3 stage was performed for *aspm-1*, and embryos from the resulting adults were fixed and either immunostained with anti–MEI-1 (red) and anti-tubulin (green), or they were immunostained with anti–ASPM-1 (red) and anti-tubulin (green). Chromosomes were stained with DAPI. Scale bars: 5 µm. (B) The ratio of the average pixel intensity in the spindle to the average pixel intensity in the cytoplasm was determined for MEI-1 staining and ASPM-1 staining in each of 14 *aspm-1(RNAi)* embryos, and the averages of these ratios are shown. The results indicate that ASPM-1 depletion was 100%. (C) *mei-1(or642)ASPM-1(RNAi)* embryos expressing GFP::tubulin and mCherry::histone were imaged in utero using a temperature-controlled stage set at 20°C. No bipolar spindles were identified in 17/17 metaphase I embryos. Scale bar: 5 µm.

between them became less regular (Figure 5A). These changes were also observed when viewed down the pole-to-pole axis (Figure 5B). The changes might be caused by merging of preexisting bundles, a loss of cross-bridging between individual microtubules within a bundle, or by assembly of new microtubules in the spaces between bundles. Wild-type microtubule bundles only intersect with other bundles at the spindle poles, whereas bundles intersected at closer spatial intervals after *mei-1(or642)* embryos were shifted to increasing temperatures (Figure 5C).

MEI-1/MEI-2 complexes bundle microtubules and preferentially sever at intersections between two microtubules in vitro

The loss of distinct pole-to-pole microtubule bundles after temperature shift of *mei-1(or642)* and the concentration of MEI-1 at spindle poles of *aspm-1(RNAi)* and wild-type spindles suggest that MEI-1/MEI-2 might directly cross-bridge or bundle microtubules in vivo. Consistent with this model, MEI-1/MEI-2 complexes but not MEI-1 alone bundled Taxol-stabilized microtubules in vitro (Figure 6, A and B). It is unlikely that in vitro microtubule bundling by MEI-1/MEI-2 is due to nonspecific aggregation, as MEI-1/MEI-2 sedimented as a single peak during sedimentation through a sucrose gradient (Figure 6C), and peak fractions from the sucrose gradient still bundled microtubules (Figure 6B). It is also unlikely that MEI-1 alone does not bundle, simply because it does not bind microtubules. Cosedimentation assays under conditions in which MEI-1/MEI-2 bundled but MEI-1 did not bundle demonstrated that similar stochiometries of MEI-1 are bound to microtubules (Figure 6D). Thus MEI-1/MEI-2 complexes can cross-bridge two microtubules in vitro.

The lengthening and bending of in vivo microtubule bundles after temperature shift of *mei-1(or642)* embryos suggested that MEI-1/MEI-2 might sever microtubules continuously within microtubule bundles in vivo to maintain a specific bundle length. For testing whether MEI-1/MEI-2 complexes can disassemble microtubules within bundles formed by MEI-1/MEI-2 complexes in vitro, microtubule bundles were first formed by mixing 1 µM MEI-1/MEI-2 with 2 µM rhodamine-labeled Taxol-stabilized microtubules in the absence of nucleotide. Bundles were then immobilized in kinesin-coated flow cells adjacent to single microtubules and perfused with 0.187 µM MEI-1/MEI-2 and ATP (Figure 6E). Because the resolution of the light microscope precludes direct imaging of severing or depolymerization of single microtubules within a bundle, the rate of change in fluorescence intensity was used to monitor microtubule disassembly within bundles. The average pixel intensity of the bundles analyzed ranged from 3 to 13 times higher than that of adjacent single microtubules. For quantification of disassembly rates, these bundles were assumed to have an average cross-section of 3–13 microtubules. Fluorescence intensity was normalized to 100% for single microtubules and normalized to 300–1300% for bundles. Bundles were disassembled at a rate of 3.15 ± 0.5%/s (n = 7 bundles in separate flow cells) as compared with adjacent single microtubules in the same flow cells, which were disassembled at a rate of 1.48 ± 0.1%/s (n = 14 microtubules in 7 flow cells). This result demonstrates that MEI-1/MEI-2 can disassemble microtubules within a bundle of microtubules cross-bridged by MEI-1/MEI-2.

Simultaneous binding of two microtubules by one katanin complex might explain the apparent recognition of microtubule intersections by katanin suggested by in vivo observations in *Arabidopsis*. In some cell types, *Arabidopsis* cortical microtubules are preferentially severed in a katanin-dependent manner at junctions created when one microtubule polymerizes past an intersecting microtubule (Wightman and Turner, 2007; Lindeboom *et al.*, 2013; Zhang *et al.*, 2013). To test whether the apparent multivalent microtubule binding by MEI-1/MEI-2 complexes might allow recognition of such intersections, we immobilized orthogonal arrays of Taxol-stabilized microtubules in kinesin-coated flow cells (Figure 6F). These orthogonal arrays were perfused with 0.187 µM MEI-1/MEI-2 complexes, and severing events were recorded by time-lapse imaging. As shown in Figure 6G, microtubules were frequently severed at the junction. To test whether the probability of severing at an intersection was greater than that at any random point on a microtubule, we determined the number of breaks per micrometer per second either at intersections or on segments of microtubule adjacent to intersections (Figure 6H). The mean rate of severing per micrometer was fivefold faster at junctions than elsewhere. Thus MEI-1/MEI-2 complexes have two previously undocumented activities: cross-bridging two microtubules and preferentially severing where two microtubules intersect.

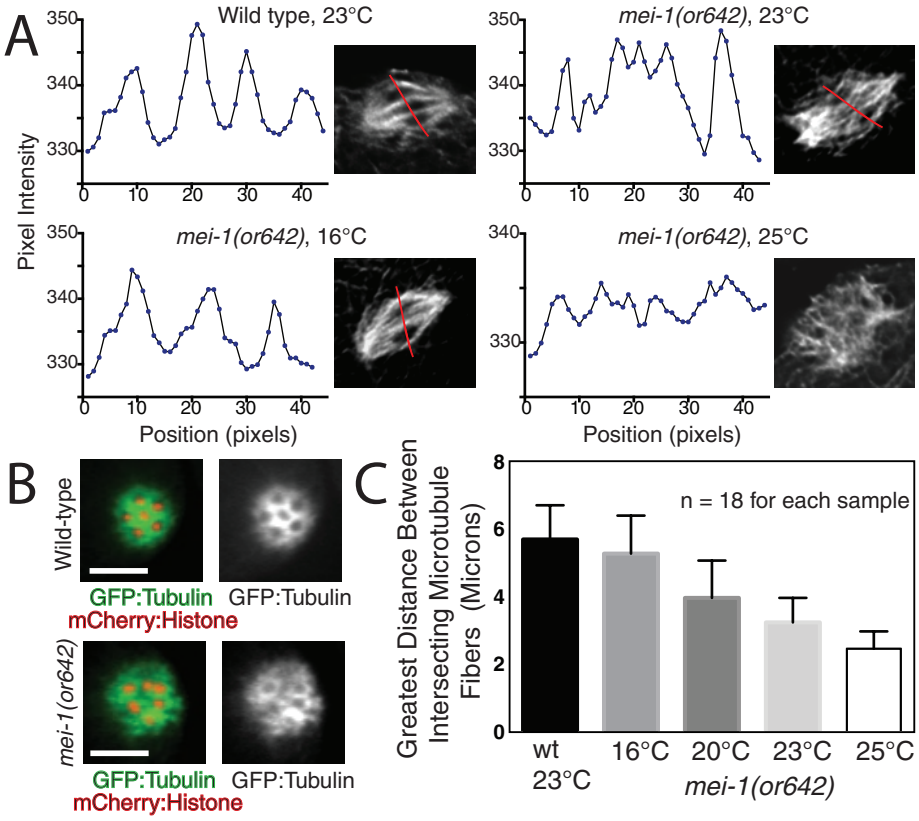

FIGURE 5: Microtubule fibers in *mei-1(or642)* spindles become less focused and are increasingly intersected with higher incubation temperatures. (A) Pixel intensities were examined across the midzone (indicated by red lines) of fixed wild-type and *mei-1(or642)* spindles. Microtubule bundles became wider and the spacing between bundles became less regular with increased temperature of incubation for the mutant. Bundle organization did not vary at different temperatures for wild type (unpublished data). (B) Cross-sections of metaphase meiotic spindles in live wild-type and *mei-1(or642)* worms expressing GFP::tubulin and mCherry::histone. The *mei-1(or642)* image was captured 10 min after a temperature increase to 23°C. Scale bars: 4 μm. (C) Increased temperature of incubation leads to a decrease in parallel microtubule organization in *mei-1(or642)* spindles. The three longest stretches of nonintersected microtubule bundle were measured in each of six fixed and stained spindles for each sample.

DISCUSSION

Katanin from multiple species severs microtubules in vitro (Hartman *et al.*, 1998; McNally *et al.*, 2000; Stoppin-Mellet *et al.*, 2007) and is required for assembly of a variety of microtubule structures in vivo (Mains *et al.*, 1990; Burk *et al.*, 2001; Sharma *et al.*, 2007; Dymek and Smith, 2012), but the mechanistic relationship between in vitro severing and katanin's in vivo functions is unclear. The finding that rapid inactivation of MEI-1 causes lengthening of a preformed spindle and the discovery of a linear relationship between spindle length and in vitro microtubule disassembly activity both support the hypothesis that continuous microtubule severing limits the length of individual microtubules within parallel/antiparallel microtubule bundles and thus limits the length of the metaphase meiotic spindle in *C. elegans*.

Other changes in spindle structure occurring after MEI-1 inactivation include movement of chromosomes off the metaphase plate, dynamic bending of microtubule bundles, loss of the discrete spacing between pole-to-pole microtubule bundles, splaying of microtubules out of the spindle, and, finally, loss of ASPM-1–positive spindle poles. These changes in spindle structure might all result from an increase in the average length of microtubules or they might result from loss of katanin's microtubule-bundling activity or its specific ability to sever intersecting microtubules.

Electron microscope tomography results indicate that microtubule bundles in wild-type meiotic spindles are composed of very short overlapping microtubules (Srayko *et al.*, 2006). Thus the length of overlap between individual microtubules within these microtubule bundles is likely determined by the microtubule sliding motors dynein, BMK-1, KLP-18, and KLP-15/16, in addition to average microtubule length, which is likely controlled by the dynamic instability regulators ZYG-9, KLP-7, and CLS-2, in addition to severing by MEI-1/MEI-2. During wild-type metaphase, bivalents are held between microtubule bundles with regular interbundle spacing (Wignall and Villeneuve, 2009; Figures 1A and 7A). If one bundle lengthens faster than an adjacent bundle after MEI-1 inactivation, this might force the longer bundle to bend acutely and also change the spacing between bundles. Bivalents might then move off the metaphase plate to maintain contacts with surrounding bundles that have the correct spacing (Figure 7A). Continued lengthening of microtubules within bundles might eventually overwhelm the sliding motors, so microtubules splay outward from the central spindle and eventually from spindle poles.

Alternatively, MEI-1/MEI-2's ability to sever preferentially at microtubule intersections and/or its cross-bridging activity might be essential to maintain parallel/antiparallel microtubule orientation within bundles. In wild-type spindles, which lack centrosomes or the branched nucleator augmin (Kamasaki *et al.*, 2013), microtubules are likely to be nucleated with random orientations. Preferential severing at intersections might prune microtubules that are not parallel or antiparallel to each other. Likewise, the cross-bridging activity of MEI-1/MEI-2 might collect randomly oriented microtubules into parallel/antiparallel bundles. Severing at intersections might also maintain the tunnels of low microtubule density in which metaphase bivalents reside, and polymerization of microtubules across these tunnels might contribute to the chromosome displacement observed upon rapid MEI-1 inactivation. MEI-1/MEI-2 is concentrated on chromosomes, and its loss from chromosomes correlates with loss of spindle bipolarity (Figure 3B and Table 3). These results suggest a feedback mechanism in which katanin on chromosomes organizes the tunnels of low microtubule density that serve to position the chromosomes.

Testing the in vivo significance of katanin's in vitro bundling activity will be critical in elucidating the mechanism of spindle assembly and maintenance. Overexpression of *Arabidopsis* katanin catalytic subunit induced microtubule bundling in vivo (Stoppin-Mellet *et al.*, 2006). Likewise, in vivo microtubule bundling in HeLa cells was induced by co-overexpression of a severing-deficient human catalytic subunit with the MEI-2–like region of a human regulatory subunit (McNally *et al.*, 2000). Although we have not found a point mutation in MEI-1

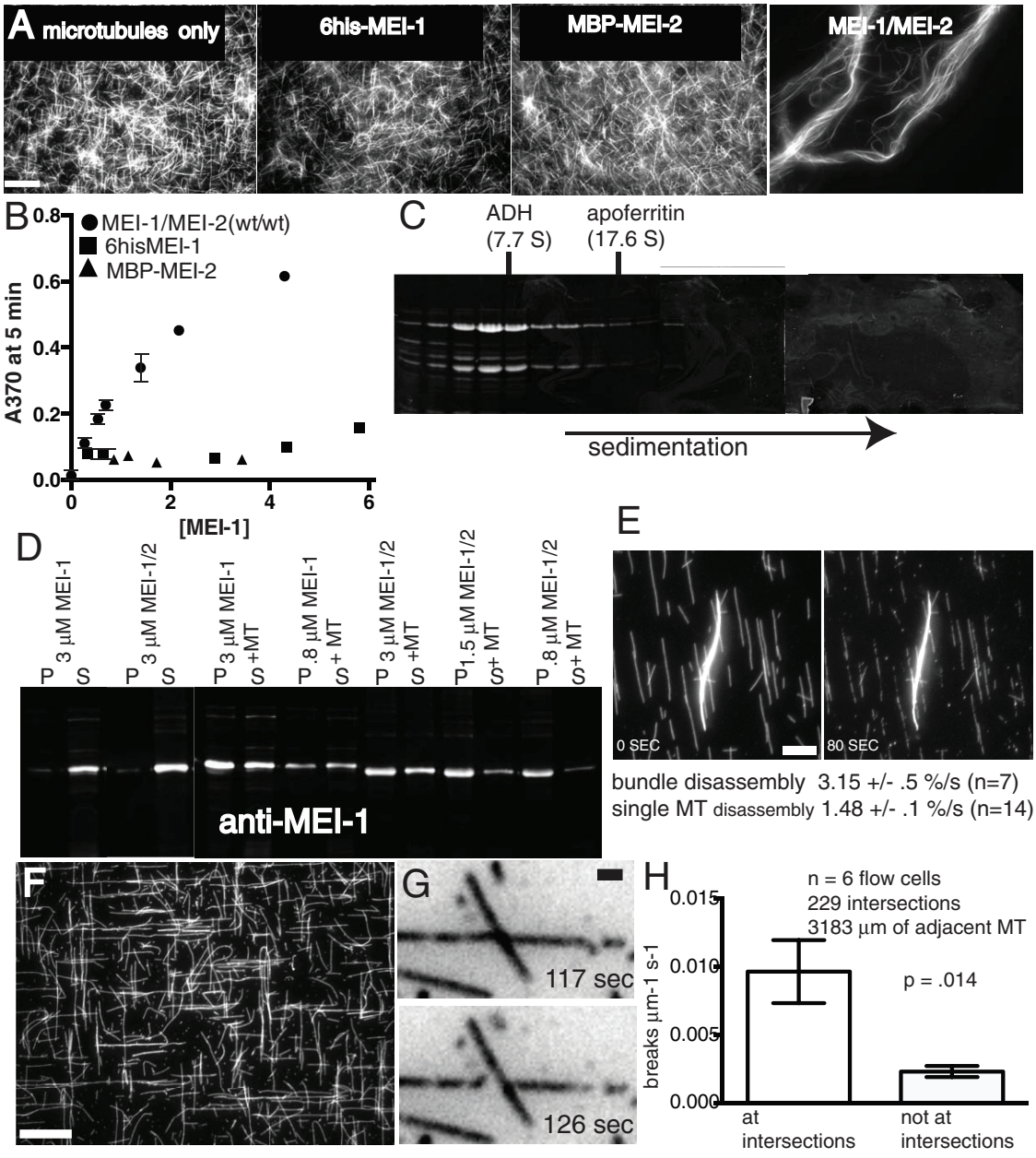

FIGURE 6: MEI-1/MEI-2 bundles microtubules and severs more frequently at microtubule intersections than on single microtubules. (A) Fluorescence images of 2 µM rhodamine microtubules incubated with 1 µM of the indicated proteins for 10 min before spreading between a slide and coverslip. (B) Light-scattering assay of microtubule bundling.Microtubules (2 µM) and the indicated proteins were mixed, and absorbance at 370 nm was recorded after 5 min. Data points with error bars are the average of three assays. Error bars indicate SEM. (C) Coomassie-stained SDS–PAGE of MEI-1/MEI-2 fractionated by velocity sedimentation on a sucrose gradient. Indicated S values are for alcohol dehydrogenase and apoferritin centrifuged in parallel. The peak fraction was used for the bundling assays in (B). (D) Anti–MEI-1 immunoblot of pellets (P) and supernatants (S) from microtubule cosedimentation assays. MT, 3 µM polymerized tubulin. (E) Time-lapse fluorescence images of a microtubule bundle formed by incubation with MEI-1/MEI-2 before immobilization next to single microtubules bound in a kinesin-coated flow cell followed by perfusion with MEI-1/MEI-2 and ATP. Disassembly rates show the average rate of decrease in fluorescence intensity of bundles and adjacent single microtubules. (F) Representative array of intersecting rhodamine-labeled microtubules formed in a crossed flow cell. (G) High-magnification time-lapse images of rhodamine microtubules exposed to 0.187 µM MEI-1/MEI-2 showing a severing event at an intersection. (H) The average rate of severing at intersections among six flow cells was 4.2 ± 0.9–fold faster than on adjacent segments of single microtubule (n = 229 intersections, 3183 µm of total adjacent microtubule length). Scale bars: (A and F) 10 µm; (G) 1 µm.

or MEI-2 that blocks in vitro microtubule bundling, both in vitro bundling and in vivo spindle assembly require both MEI-1 and MEI-2.

Both microtubule bundling and recognition of microtubule intersections require at least two microtubule-binding sites in the same molecule, preferably with a geometry that favors binding two different microtubules rather than two tubulin dimers within the same microtubule. Considerable indirect evidence supports a model in which katanin forms a transient radial hexamer with six N-terminal

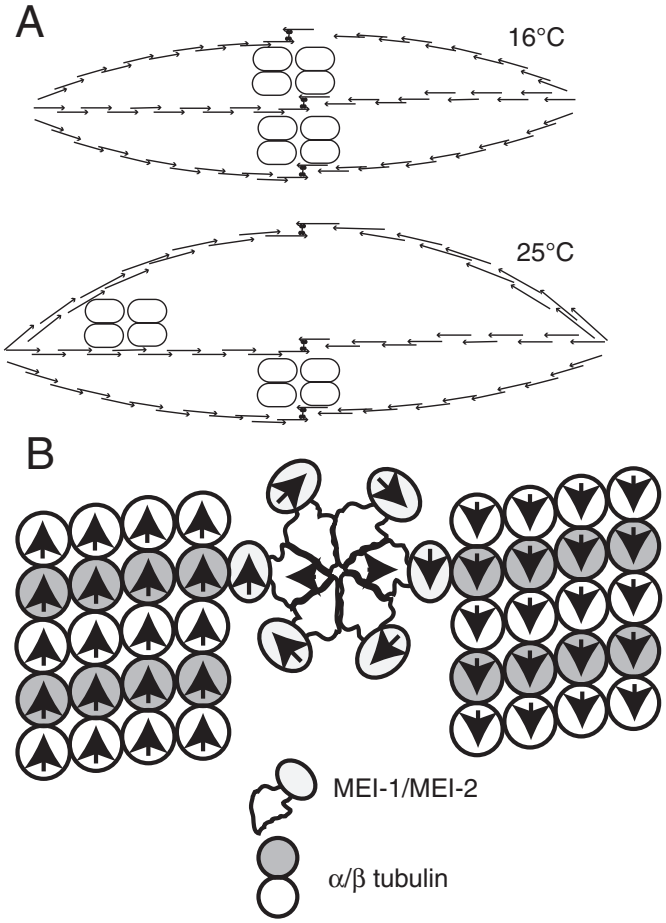

FIGURE 7: Models for chromosome displacement after katanin inactivation and a mechanism for microtubule bundling. (A) Cartoon of a *mei-1(ts)* metaphase I spindle at permissive temperature. Bivalents are positioned between bundles composed of overlapping short microtubules. After a shift to nonpermissive temperature, microtubules lengthen, causing microtubule bundles to lengthen. The top bundle lengthens faster than the lower bundles, causing the top bundle to bend outward, changing the spacing between bundles. One bivalent moves to maintain lateral contact with the bending bundle. (B) Cartoon of a MEI-1/MEI-2 hexameric ring between two antiparallel microtubules. Arrows indicate the symmetry of the protein structures. Only four tubulin protofilaments are drawn for simplicity.

microtubule-binding domains extending radially outward from a central AAA ring (Hartman *et al.*, 1998; Hartman and Vale, 1999; Roll-Mecak and Vale, 2008; Roll-Mecak and McNally, 2010). Because tubulin subunits within a microtubule have linear rather than radial symmetry, two microtubule-binding domains within the same transient hexamer might be able to cross-bridge two different microtubules but not bind to two tubulin dimers within the same microtubule (Figure 7B). Elucidating the structure of a microtubule-bound MEI-1/MEI-2 oligomer may allow the design of separation-of-function mutants that could reveal the relative importance of severing and bundling in vivo.

MATERIALS AND METHODS

Purification of MEI-1/MEI-2 complexes

Two alternatively spliced MEI-1 mRNAs distinguished by a three-codon insertion have been reported (Clark-Maguire and Mains, 1994b). The short isoform was chosen for this study because it expresses at higher levels in *Escherichia coli* and because the three-amino-acid insertion in the long isoform is not present in katanin catalytic subunits from other organisms. An *E. coli* codon-optimized gene encoding the short isoform of *C. elegans* MEI-1 was synthesized by Genscript (Piscataway, NJ) and inserted into pET28a (6his tag, kanamycin resistant, ColE1 ori) and pCDF-Duet (untagged, streptomycin resistant, CDF ori). An MEI-2 cDNA was cloned into pMAL-CRI with a TEV (tobacco etch virus protease) cleavage site (MBP [maltose-binding protein] tag, ampicillin resistant, ColE1 origin). Point mutants of MEI-1 or MEI-2 were synthesized by Genscript and confirmed by sequencing. *E. coli* BL21DE3 was cotransformed with pCDF-Duet-MEI-1 and pMAL-CRI-TEV-MEI-2 or pet28-MEI-1 alone. One-liter cultures were grown to log phase at 37°C, shifted to 16°C, and then induced with isopropyl β-D-1-thiogalactopyranoside. Fresh cultures were harvested by centrifugation; resuspended in 100 ml lysis buffer with 40 mM HEPES (pH 7.5), 500 mM NaCl, 2 mM $MgCl_2$, 10% glycerol with protease inhibitors; microfluidized; and centrifuged at 10,000 × *g*. Supernatants were flash frozen and stored at −80°C. Fifty milliliters of 6his-MEI-1 supernatant was brought to 30 mM imidazole, applied to a 5-ml bed volume of Ni^{2+}-charged His-Bind resin (EMD Millipore, Billerica, MA), washed with lysis buffer, and then eluted with 40 mM HEPES (pH 7.5), 375 mM NaCl, 250 mM imidazole, 2 mM $MgCl_2$, 10% glycerol. Fifty milliliters of MEI-1/MBP-TEV-MEI-2 supernatant was applied to a 5-ml amylose resin (New England Biolabs, Ipswich, MA) column and washed with lysis buffer. For TEV protease digestion, 200 μg TEV protease was diluted in 6 ml of lysis buffer and flowed through the column. Digestions were carried out in the column for 2 h at 16 or 22°C; this was followed by elution with lysis buffer at 4°C. For determination of protein concentrations, MEI-1/MEI-2 preparations were resolved by SDS–PAGE, along with bovine serum albumin (BSA) standards, and stained with Coomassie Brilliant Blue G250; infrared fluorescence was quantified with a LI-COR Odyssey (LI-COR Biosciences, Lincoln, NE). Concentrations of MEI-1 were calculated by comparison with the infrared fluorescence of the BSA standards and corrected for molecular weight. The stoichiometry of MEI-1:MEI-2 did not vary among mutants (Figure 2G). For wild type and each mutant, a second plasmid preparation was sequenced to verify the mutation, and the newly confirmed DNA preparation was transformed into BL21DE3 and used for a second protein purification. Data in Table 1 are averaged from assays using both preparations.

Microtubule-severing assays

The K560 fragment of human G234A kinesin was first flowed into a flow cell composed of a slide, coverslip, and two strips of Scotch double-sided tape. Kinesin-free surfaces were blocked with 5% Pluronic F150 in PME (100 mM PIPES 6.8, 1 mM $MgCl_2$, 1 mM ethylene glycol tetraacetic acid [EGTA]) and then washed with PME. Taxol-stabilized microtubules (0.1 μM) assembled from tetramethylrhodamine–labeled, MAP (microtubule-associated protein)-free porcine brain tubulin were allowed to adhere in the flow cell, and then nonadherent microtubules were washed out with assay buffer (25 mM HEPES, pH 7.5, 10% glycerol, 2 mM $MgSO_4$, 0.5 mM EGTA). For time-lapse assays, adhered microtubules were first perfused with assay buffer with 20 μM Taxol, 1 mM ATP, and an oxygen-scavenging system composed of catalase, glucose oxidase, glucose, and β-mercaptoethanol. The flow cell was placed on the microscope, and microtubules were quickly brought into focus with brief illumination. Forty microliters of MEI-1/MEI-2 diluted into assay buffer with 20 μM Taxol, 1 mM ATP, and oxygen scavengers was quickly flowed through the 10-μl flow cell, and shuttered time-lapse acquisition was initiated. All dilutions of MEI-1/MEI-2 from 500 mM NaCl

stocks were adjusted to 50 mM NaCl final concentration. All preparations of MEI-1/MEI-2 used for quantitative analysis were freeze thawed once before purification and once after purification. Crossed microtubules were made as follows: flow cells were assembled from a slide and coverslip with four squares of double-stick tape at the four corners of the coverslip; after microtubules were flowed in one direction and allowed to adhere, a second solution of microtubules was flowed in at 90° and allowed to adhere, and free microtubules were then washed out.

Image acquisition was with a Nikon Microphot SA upright microscope equipped with a 60× Plan-Apo 1.4 objective; heat, UV, and neutral density filters; an electronic shutter in the excitation path; and a QImaging Retiga EXi fast 1394 CCD camera (Burnaby, Canada) controlled by Ivision software (Biovision Technologies, Exton, PA). For the assays reported in Table 1 and Figures 2 and 6E, images were captured at 10-s intervals using 2 × 2 binning to minimize photodamage. For the assays reported in Figure 6, F–H, images were captured at 3-s intervals with no binning to allow unambiguous scoring of individual severing events.

Microtubule-bundling assays

For qualitative bundling assays (Figure 6A), MEI-1/MEI-2 complexes were diluted in lysis buffer adjusted to a final salt concentration of 150 mM NaCl and then centrifuged in a TLA100 rotor for 20 min at 60,000 rpm. Supernatants were then mixed with tetramethyl-rhodamine–labeled microtubules before a 3-µl aliquot was spread between a slide and coverslip for imaging. For quantitative light-scattering assays (Figure 6B), MEI-1/MEI-2 complexes were further purified by Ni^{2+} chelate chromatography (Figure 2A) and velocity sedimentation through a 5–50% wt/vol sucrose step gradient in 40 mM HEPES (pH 7.5), 150 mM NaCl, 2 mM $MgCl_2$ in a Beckman SW41 rotor centrifuged at 35,000 rpm for 14 h (Figure 6C). The peak fraction shown in Figure 6C was diluted in the same buffer without sucrose and rapidly mixed with unlabeled, Taxol-stabilized, MAP-free, porcine brain microtubules in a 100-µl quartz cuvette in a Beckman Coulter DU530 UV-visible spectrophotometer. Absorbance at 370 nm was recorded at 5-s intervals. MEI-1/MEI-2 complexes, 6his-MEI-1, and MBP-MEI-2 exhibited minimal light scattering when incubated without microtubules through the 5-min time point reported in Figure 6B (unpublished data), supporting the interpretation that the increased light scattering is caused by microtubule bundling rather than aggregation of MEI-1/MEI-2.

Microtubule cosedimentation

MEI-1 or MEI-1/MEI-2 preparations were diluted to 150 mM NaCl, 40 mM HEPES (pH 7.5), 2 mM $MgCl_2$ and centrifuged at 60,000 rpm in a TLA100 rotor for 20 min before being mixed with either Taxol-stabilized microtubules polymerized from porcine brain tubulin in PME or with an equivalent volume of PME. One hundred–microliter reactions were incubated at 22°C for 5 min and then loaded onto a cushion composed of 30% glycerol, 150 mm NaCl, 40 mM HEPES (pH 7.5), 2 mM $MgCl_2$, 20 µM Taxol before being centrifuged at 60,000 rpm for 20 min in a TLA100 rotor. Supernatants were removed, and pellets were resuspended in 1% SDS. Equivalent aliquots of pellets and supernatants were resolved by SDS–PAGE and stained with Coomassie Brilliant Blue G-250.

C. elegans strains

Strains were cultured according to standard procedures (Brenner, 1974). For fixed immunofluorescence imaging, wild type was N2 Bristol; for live fluorescence imaging, wild type indicates the integrated GFP::tubulin and mCherry::histone strain FM125 *ruIs57[pAZ147:pie-1/β-tubulin::GFP; unc-119(+)]; itIs37[pie-1::mCherry::H2B; unc-119(+)]*. The *mei-1(or642)* strain EU1334 was used for fixed immunofluorescence imaging; for live fluorescence imaging, GFP::tubulin and mCherry::histone from FM125 were crossed into EU1334 to generate the strain FM240 *mei-1(or642) I; ruIs57; itIs37*. Additional strains used were FM38, *mei-1(ct46) unc-13(e1091) I; ruIs57*; FM24, *mei-1(ct46) mei-2(sb121) unc-13(e1091) I; ruIs57*; HR1549, *mei-2(sb121) unc-13(e1091) unc-29(e1072) I; uIs57[pAZ147:pie1/GFP::tbb-2]; itIs37*; HR1557, *mei-1(ct46) mei-2(sb121) unc-13(e1091) dpy-5(e61) I; ruIs57; itIs37*; HR1548, *mei-1(ct46ct82) unc-29(e1072) I/hT2 [bli-49(e9370) let-9(q7820) qIs48] III*; FM12, *mei-2(ct98) I; ruIs57*; FM10, *mei-1(ct46ct101) unc-13(e1091) daf-8(e1393)/hT2[bli-4(e937) let(h661)] I; hT2/+ III; ruIs57*; HR1391, *mei-2(ct102) unc-13(e1091)/hT2[bli-4(e937) let(h661)] I*; and BW1036, *dpy-5(e61) mei-1(b284) unc-29(e1072)/unc-13(e1091) lin-11(n566) I*. N2, FM125, and BW1036 were maintained at 20°C; all temperature-sensitive mutants were maintained at 16°C. For measurement of spindle lengths at restrictive temperatures, strains were shifted to 25°C for 24 h before imaging.

mei-2(sb121) was isolated as a dominant suppressor of *mei-1(ct46)* (Clandinin and Mains, 1993). After 10 outcrosses, we found that the strain *mei-1(ct46sb16)* (McNally and McNally, 2011) contained an R233Q lesion in *mei-2* rather than the *sb16* mutation in *mei-1*. An *mei-1(ct46) mei-2(sb121)* double mutant reconstructed from the outcrossed *mei-2(sb121)* had the same long-spindle phenotype (Table 2) previously observed in the original suppressor strain (McNally and McNally, 2011). At 25°C, outcrossed *sb121* showed 95% hatching, while *mei-2(sb121) mei-1(ct46)* showed 87% hatching (vs. 0% for *mei-1(ct46)*. The suppression of *ct46* cosegregated with the *sb121* lesion in 21/21 crossovers in the 2 cM region (*dpy-5* to *unc-13*) that flanks *mei-2*.

RNA interference

mat-1 and *aspm-1* RNAi experiments were carried out by feeding bacteria (HT115) induced to express double-stranded RNA corresponding to each gene as described (Kamath *et al.*, 2001; Timmons *et al.*, 2001; Source Bioscience, Nottingham, United Kingdom). L3 hermaphrodites were transferred to RNAi plates and allowed to feed on the RNAi bacterial lawn for 40–44 h. For metaphase-arrested embryos, FM125 or FM240 worms were fed at 16°C; for ASPM-1 depletion, N2 worms were fed at 20°C.

Live imaging

Briefly, adult hermaphrodites were anesthetized with tricaine/tetramisole and immobilized between a coverslip and an agarose pad on a slide as previously described (Yang *et al.*, 2003). Time-lapse imaging was done on a Perkin Elmer-Cetus (Waltham, MA) Ultraview spinning-disk confocal microscope utilizing an Olympus (Center Valley, PA) 60× Plan-Apo 1.4 objective and a Hamamatsu (Hamamatsu City, Japan) Orca ER CCD camera. For imaging of meiotic spindles, *mei-1(or642)*, GFP::tubulin, mCherry::histone worms or GFP::tubulin, mCherry::histone control worms were mounted and placed on a 20/20 Technology BC-110 Bionomic Controller stage initially set at 16°C. A +1 embryo (the newly fertilized embryo immediately next to the spermatheca) with a metaphase-arrested spindle was then identified, an initial image was captured, and the stage was heated to 25°C. The spindles were visualized by capturing pairs of single focal-plane red and green fluorescence images at 10-s intervals. After completion of filming, the temperature of the immersion oil was measured with an Omega Engineering HH81 digital thermometer to ensure that the sample was at 25°C.

Immunofluorescence

For imaging of fixed embryos from *mei-1(or642)* worms, adult hermaphrodites were washed in Petri dishes that had been placed in a 20/20 Technology BC-110 Bionomic Controller and containing 0.8X egg buffer at the appropriate temperatures. The worms were quickly transferred to polylysine-coated glass slides (Superfrost Plus; Thermo Fisher Scientific, Lafayette, CO), excess liquid was wicked away, a coverslip was gently applied to extrude embryos from the mother, and the slides were submerged into liquid nitrogen for 10 min. After removal from liquid nitrogen, the coverslips were quickly flicked off, and the slides were submerged in –20°C MeOH for 25 min. Slides were washed twice for 10 min in phosphate-buffered saline (PBS) and once for 15 min in PBS containing 0.05% Tween 20 (PBST). Slides were preblocked in 4% BSA in PBST for 45 min at room temperature; this was followed by overnight incubation with primary antibodies at 4°C. Slides were washed twice for 10 min in PBS and once for 15 min in PBST and then incubated with secondary antibodies and 4′,6-diamidino-2-phenylindole (DAPI) for 1 h at room temperature. Slides were washed twice for 10 min in PBS and once for 15 min in PBST and then mounted with a coverslip and 1,4-diazabicyclo[2.2.2]octane/Mowiol. Primary antibodies were diluted in PBST and 4% BSA in the following ratios: 1:100 anti–MEI-1 (this study), 1:100 anti–ASPM-1 (van der Voet *et al.*, 2009), and 1:200 DM1α anti-tubulin (Sigma-Aldrich, St. Louis, MO). The secondary antibodies, Alexa Fluor 488 goat anti–rabbit immunoglobulin G (IgG) and Alexa Fluor 594 goat anti-mouse IgG (Molecular Probes, Eugene, OR) were diluted 1:200 in PBST. DAPI staining was used to visualize DNA. Stained embryos were imaged using an Olympus IX71 inverted microscope equipped with a 60× Plan-Apo 1.42 numerical aperture objective, an Olympus DSU (disk-scanning unit), and a Hamamatsu Orca R2 deep-cooled C10600-10B digital mono CCD camera. Excitation light was regulated with a Sutter shutter, a Sutter Lambda 10–3 controller, and MetaMorph imaging software through a Sutter excitation filter wheel. Z stacks of images were taken in 0.20-μm step size. Images were deconvolved using Huygens Professional X11 software (Scientific Volume Imaging, Hilversum, Netherlands).

ACKNOWLEDGMENTS

Some strains were obtained from the Caenorhabditis Genetics Center (University of Minnesota, Minneapolis, MN), which is funded by the National Institutes of Health (NIH) Office of Research Infrastructure Programs (P40 OD010440). We thank Sander van den Heuvel for anti–ASPM-1 antibodies and Jon Scholey for use of his confocal microscope. This work was supported by funding from the National Institute of General Medical Sciences (grant 1R01GM-079421 to F.J.M.), by the Canadian Institutes of Health Research (to P.E.M.), and by an NIH training grant (5T32GM007377) and a Floyd and Mary Schwall Fellowship (to D.B.C.).

REFERENCES

Brenner S (1974). The genetics of *Caenorhabditis elegans*. Genetics 77, 71–94.

Burk DH, Liu B, Zhong R, Morrison WH, Ye ZH (2001). A katanin-like protein regulates normal cell wall biosynthesis and cell elongation. Plant Cell 13, 807–827.

Clandinin TR, Mains PE (1993). Genetic studies of *mei-1* gene activity during the transition from meiosis to mitosis in *Caenorhabditis elegans*. Genetics 134, 199–210.

Clark-Maguire S, Mains PE (1994a). Localization of the *mei-1* gene product of *Caenorhabditis elegans*, a meiotic-specific spindle component. J Cell Biol 126, 199–209.

Clark-Maguire S, Mains PE (1994b). *mei-1*, a gene required for meiotic spindle formation in *Caenorhabditis elegans*, is a member of a family of ATPases. Genetics 136, 533–546.

Davis ES, Wille L, Chestnut BA, Sadler PL, Shakes DC, Golden A (2002). Multiple subunits of the *Caenorhabditis elegans* anaphase-promoting complex are required for chromosome segregation during meiosis I. Genetics 160, 805–813.

Dymek EE, Lefebvre PA, Smith EF (2004). PF15p is the *Chlamydomonas* homologue of the katanin p80 subunit and is required for assembly of flagellar central microtubules. Eukaryotic Cell 3, 870–879.

Dymek EE, Smith EF (2012). PF19 encodes the p60 catalytic subunit of katanin and is required for assembly of the flagellar central apparatus in *Chlamydomonas*. J Cell Sci 125, 3357–3366.

Eckert T, Le DT, Link S, Friedmann L, Woehlke G (2012). Spastin's microtubule-binding properties and comparison to katanin. PLoS One 7, e50161.

Gomes JE, Tavernier N, Richaudeau B, Formstecher E, Boulin T, Mains PE, Dumont J, Pintard L (2013). Microtubule severing by the katanin complex is activated by PPFR-1-dependent MEI-1 dephosphorylation. J Cell Biol 202, 431–439.

Hartman JJ, Mahr J, McNally K, Okawa K, Iwamatsu A, Thomas S, Cheesman S, Heuser J, Vale RD, McNally FJ (1998). Katanin, a microtubule-severing protein, is a novel AAA ATPase that targets to the centrosome using a WD40-containing subunit. Cell 93, 277–287.

Hartman JJ, Vale RD (1999). Microtubule disassembly by ATP-dependent oligomerization of the AAA enzyme katanin. Science 286, 782–785.

Kamasaki T, O'Toole E, Kita S, Osumi M, Usukura J, McIntosh JR, Goshima G (2013). Augmin-dependent microtubule nucleation at microtubule walls in the spindle. J Cell Biol 202, 25–33.

Kamath RS, Martinez-Campos M, Zipperlen P, Fraser AG, Ahringer J (2001). Effectiveness of specific RNA-mediated interference through ingested double-stranded RNA in *Caenorhabditis elegans*. Genome Biol 2, RESEARCH0002.

Lindeboom JJ, Nakamura M, Hibbel A, Shundyak K, Gutierrez R, Ketelaar T, Emons AM, Mulder BM, Kirik V, Ehrhardt DW (2013). A mechanism for reorientation of cortical microtubule arrays driven by microtubule severing. Science 342, 1245533.

Mains PE, Kemphues KJ, Sprunger SA, Sulston IA, Wood WB (1990). Mutations affecting the meiotic and mitotic divisions of the early *Caenorhabditis elegans* embryo. Genetics 126, 593–605.

McNally K, Audhya A, Oegema K, McNally FJ (2006). Katanin controls mitotic and meiotic spindle length. J Cell Biol 175, 881–891.

McNally KP, Bazirgan OA, McNally FJ (2000). Two domains of p80 katanin regulate microtubule severing and spindle pole targeting by p60 katanin. J Cell Sci 113, 1623–1633.

McNally KP, McNally FJ (2011). The spindle assembly function of *Caenorhabditis elegans* katanin does not require microtubule-severing activity. Mol Biol Cell 22, 1550–1560 [correction published in Mol Biol Cell (2012). 23, 4472].

McNally FJ, Vale RD (1993). Identification of katanin, an ATPase that severs and disassembles stable microtubules. Cell 75, 419–429.

O'Rourke SM *et al.* (2011). A survey of new temperature-sensitive, embryonic-lethal mutations in *C. elegans*: 24 alleles of thirteen genes. PLoS One 6, e16644.

Roll-Mecak A, McNally FJ (2010). Microtubule-severing enzymes. Curr Opin Cell Biol 22, 96–103.

Roll-Mecak A, Vale RD (2008). Structural basis of microtubule severing by the hereditary spastic paraplegia protein spastin. Nature 451, 363–367.

Sharma N, Bryant J, Wloga D, Donaldson R, Davis RC, Jerka-Dziadosz M, Gaertig J (2007). Katanin regulates dynamics of microtubules and biogenesis of motile cilia. J Cell Biol 178, 1065–1079.

Sonneville R, Gönczy P (2004). Zyg-11 and cul-2 regulate progression through meiosis II and polarity establishment in *C. elegans*. Development 131, 3527–3543.

Srayko M, Buster DW, Bazirgan OA, McNally FJ, Mains PE (2000). MEI-1/MEI-2 katanin-like microtubule severing activity is required for *Caenorhabditis elegans* meiosis. Genes Dev 14, 1072–1084.

Srayko M, O'Toole ET, Hyman AA, Muller-Reichert T (2006). Katanin disrupts the microtubule lattice and increases polymer number in *C. elegans* meiosis. Curr Biol 16, 1944–1949.

Stoppin-Mellet V, Gaillard J, Timmers T, Neumann E, Conway J, Vantard M (2007). *Arabidopsis* katanin binds microtubules using a

multimeric microtubule-binding domain. Plant Physiol Biochem 45, 867–877.
Stoppin-Mellet V, Gaillard J, Vantard M (2006). Katanin's severing activity favors bundling of cortical microtubules in plants. Plant J 46, 1009–1017.
Timmons L, Court DL, Fire A (2001). Ingestion of bacterially expressed dsRNAs can produce specific and potent genetic interference in *Caenorhabditis elegans*. Gene 263, 103–112.
van der Voet M, Berends CW, Perreault A, Nguyen-Ngoc T, Gönczy P, Vidal M, Boxem M, van den Heuvel S (2009). NuMA-related LIN-5, ASPM-1, calmodulin and dynein promote meiotic spindle rotation independently of cortical LIN-5/GPR/Gα. Nat Cell Biol 11, 269–277.
Wightman R, Turner SR (2007). Severing at sites of microtubule crossover contributes to microtubule alignment in cortical arrays. Plant J 52, 742–751.
Wignall SM, Villeneuve AM (2009). Lateral microtubule bundles promote chromosome alignment during acentrosomal oocyte meiosis. Nat Cell Biol 11, 839–844.
Yang HY, McNally K, McNally FJ (2003). MEI-1/katanin is required for translocation of the meiosis I spindle to the oocyte cortex in *C. elegans*. Dev Biol 260, 245–259.
Zhang Q, Fishel E, Bertroche T, Dixit R (2013). Microtubule severing at crossover sites by katanin generates ordered cortical microtubule arrays in *Arabidopsis*. Curr Biol 23, 2191–2195.